Journal of Zhejiang University SCIENCE A
ISSN 1673-565X (Print); ISSN 1862-1775 (Online)
www.zju.edu.cn/jzus; www.springerlink.com
E-mail: jzus@zju.edu.cn

Approach for analyzing the ultimate strength of concrete filled steel tubular arch bridges with stiffening girder

ZHANG Zhi-cheng[†], XIE Xu[†‡], ZHANG He, CHEN Heng-zhi

(*Department of Civil Engineering, Zhejiang University, Hangzhou 310027, China*)

[†]E-mail: jszzc@zju.edu.cn; xiexu@zju.edu.cn

Received Nov. 2, 2006; revision accepted Jan. 18, 2007

Abstract: A convenient approach is proposed for analyzing the ultimate load carrying capacity of concrete filled steel tubular (CFST) arch bridge with stiffening girders. A fiber model beam element is specially used to simulate the stiffening girder and CFST arch rib. The geometric nonlinearity, material nonlinearity, influence of the construction process and the contribution of prestressing reinforcement are all taken into consideration. The accuracy of this method is validated by comparing its results with experimental results. Finally, the ultimate strength of an abnormal CFST arch bridge with stiffening girders is investigated and the effect of construction method is discussed. It is concluded that the construction process has little effect on the ultimate strength of the bridge.

Key words: Ultimate strength, Concrete filled steel tubular (CFST) arch bridge, Stiffening girder, Fiber model beam element, Construction process

doi:10.1631/jzus.2007.A0682 **Document code:** A **CLC number:** TU31

INTRODUCTION

With the increasing applications of concrete filled steel tubular (CFST) structures in civil engineering in China, arch bridges have become one of the competitive styles in moderate span or long span bridges. Taking the Fuxing Bridge in Hangzhou (Zhao *et al*., 2004), and Wushan Bridge in Chongqing (Zhang *et al*., 2003), China, as representatives, the structural configuration, the span and construction scale of such bridges have surpassed those of existing CFST arch bridges in the world. Therefore, it is of great importance to enhance the theoretical level in the design of CFST arch bridges for safety and economy.

The calculation of ultimate bearing capacity is a significant issue in design of CFST arch bridges. As an arch structure is primarily subjected to compressive forces, the ultimate strength of CFST arch bridge is determined by the stability requirement. A number of theoretical studies were conducted in the past to investigate the stability and load-carrying capacity of CFST arch bridges. Zeng *et al*.(2003) studied the load capacity of CFST arch bridge using a composite beam element, involving geometric and material nonlinearity. Zhang *et al*.(2006) derived a tangent stiffness matrix for spatial CFST pole element to consider the geometric and material nonlinearities under large displacement by co-rotational coordinate method. Xie *et al*.(2005) proposed a numerical method to determine the ultimate strength of CFST arch bridges and revealed that the effect of the constitutive relation of confined concrete is not significant. Hu *et al*.(2006) investigated the effect of Poisson's ratio of core concrete on the ultimate bearing capacity of a long span CFST arch bridge and found that the bearing capacity is enhanced by 10% if the Poisson's ratio is variable. On the other hand, many experimental studies on the ultimate strength of naked CFST arch rib or CFST arch bridge model had been conducted. Experimental studies on CFST arch rib under in-plane and out-of-plane loads were carried out by Chen and Chen

‡ Corresponding author

(2000) and Chen *et al*.(2006), showing that the geometrical nonlinearity was significant for the out-of-plane strength and less significant for the in-plane strength. Cui *et al*.(2004) introduced a global model test of a CFST arch bridge with span of 308 m, and suggested that the influence of initial stress should be considered.

The above papers mainly focused on the ultimate strength of CFST naked arch ribs or CFST arch bridges with floating deck. No attempt was made to study the ultimate strength of CFST arch bridges with stiffening girders whose nonlinear behavior and CFST arch should be simulated due to the redistribution of inner forces between arch ribs and stiffening girders. In general, stiffening girders can be classified into steel girder, PC (prestressing concrete) girder and steel-concrete combination girder. It is most difficult to simulate the nonlinear behavior of PC girder, due to the influence of prestressing reinforcement. In contrast to steel or steel-concrete combination beam, the prestressing reinforcements in PC girders not only offer strength and stiffness directly, but their tension greatly affects the stiffness and distribution of the initial forces in the structure.

The aims of this paper are (1) to present an elastic-plastic analysis of the ultimate strength of CFST arch bridge with arbitrary stiffening girders; (2) to study the ultimate load-carrying capacity of a complicated CFST arch bridge with abnormal arch ribs and PC stiffening girders; and (3) to investigate the effect of construction methods on the ultimate strength of the structure.

ANALYTICAL THEORY

Elasto-plastic large deformation of PC girder element

The elasto-plastic large deformation analysis of PC beam elements is based on the following fundamental assumptions:

(1) A plane section originally normal to the neutral axis always remains a plane and normal to the neutral axis during deformation;

(2) The shear deformation due to shear stress is neglected;

(3) The Saint-Venant torsional principle holds in the elasto-plastic stage;

(4) The effect of shear stress on the stress-strain relationship is ignored.

The cross-section of a PC box girder with one symmetric axis is depicted in Fig.1, where, G and s denote the geometry center and the shear center respectively. According to the first and the third assumptions listed above, the displacement increments of point $A(x,y)$ in the section can be expressed in terms of the displacement increments at the geometry center and the shear center as

$$\begin{cases}\Delta W(x,y,z)=\Delta w_G-x\Delta u_s'-y\Delta v_s',\\ \Delta U(x,y,z)=\Delta u_s-(y-y_s)\Delta\theta_z,\\ \Delta V(x,y,z)=\Delta v_s+x\Delta\theta_z,\end{cases} \tag{1}$$

in which Δw_G is the longitudinal displacement increment of point G, Δu_s and Δv_s are the displacement increments of point s in the x- and y-directions respectively, and $\Delta\theta_z$ is the increment of torsional angle. The linear normal strain increment $\Delta\varepsilon_{\mathrm{L}}$, nonlinear normal strain increment $\Delta\varepsilon_{\mathrm{N}}$ and shear strain increment $\Delta\gamma$ of point $A(x,y)$ in the cross-section can be expressed with updated Lagrangian formulation as

$$\begin{cases}\Delta\varepsilon_{\mathrm{L}}=\Delta w_G'-x\Delta u_s''-y\Delta v_s'',\\ \Delta\varepsilon_{\mathrm{N}}=\dfrac{1}{2}\left(\dfrac{\partial\Delta U}{\partial z}\right)^2+\dfrac{1}{2}\left(\dfrac{\partial\Delta V}{\partial z}\right)^2\\ \qquad\quad=\dfrac{1}{2}\left[\Delta u_s'-(y-y_s)\Delta\theta_z'\right]^2+\dfrac{1}{2}\left(\Delta v_s'+x\Delta\theta_z'\right)^2,\\ \Delta\gamma=K_{\mathrm{tor}}\Delta\theta_z',\end{cases} \tag{2}$$

where K_{tor} is the coefficient factor which is related to the geometry shape of the girder cross-section.

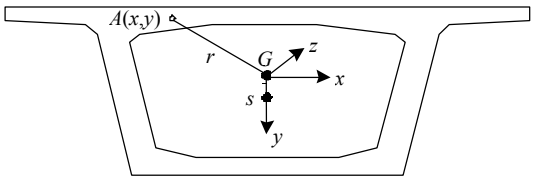

Fig.1 Cross-section of a PC box girder

Similar to 3D elastic beam theory, the displacement increment of the girder can be expressed in terms of the nodal displacement increments as

$$\begin{cases}\Delta w_G = N_{w1}\Delta w_{Gi} + N_{w2}\Delta w_{Gj},\\ \Delta\theta_z = N_{w1}\Delta\theta_{zi} + N_{w2}\Delta\theta_{zj},\\ \Delta u_s = N_1\Delta u_{si} + N_2\Delta u'_{si} + N_3\Delta u_{sj} + N_4\Delta u'_{sj},\\ \Delta v_s = N_1\Delta v_{si} + N_2\Delta v'_{si} + N_3\Delta v_{sj} + N_4\Delta v'_{sj},\end{cases} \tag{3}$$

where the shape functions are

$$\begin{cases}N_{w1} = 1 - z/L,\\ N_{w1} = z/L,\\ N_1 = 1 - 3(z/L)^2 + 2(z/L)^3,\\ N_2 = z - 2z^2/L + z^3/L^2,\\ N_3 = 3(z/L)^2 - 2(z/L)^3,\\ N_4 = -z^2/L + z^3/L^2,\end{cases} \tag{4}$$

in which L denotes the element length, and z is the axial coordinate of the local coordinate system of an element. Then, the displacement vector of any section of the element can be written as

$$\Delta\boldsymbol{u} = \boldsymbol{N}\Delta\boldsymbol{u}^{\mathrm{e}}, \tag{5}$$

where $\Delta\boldsymbol{u}$ is the displacement vector of any section of the beam element, $\boldsymbol{N}$ is the shape function matrix and $\Delta\boldsymbol{u}^{\mathrm{e}}$ is the displacement vector of the element node. They are respectively expressed as

$$\Delta\boldsymbol{u} = [\Delta w_G \quad \Delta u_s \quad \Delta u'_s \quad \Delta v_s \quad -\Delta v'_s \quad \Delta\theta_z]^{\mathrm{T}}, \tag{6}$$

$$\boldsymbol{N} = \begin{bmatrix} N_{w1} & 0 & 0 & 0 & 0 & 0\\ 0 & N_1 & N_2 & 0 & 0 & 0\\ 0 & N'_1 & N'_2 & 0 & 0 & 0\\ 0 & 0 & 0 & N_1 & -N_2 & 0\\ 0 & 0 & 0 & -N'_1 & N'_2 & 0\\ 0 & 0 & 0 & 0 & 0 & N'_{w1}\end{bmatrix}$$
$$\begin{bmatrix} N_{w2} & 0 & 0 & 0 & 0 & 0\\ 0 & N_3 & N_4 & 0 & 0 & 0\\ 0 & N'_3 & N'_4 & 0 & 0 & 0\\ 0 & 0 & 0 & N_3 & -N_4 & 0\\ 0 & 0 & 0 & -N'_3 & N'_4 & 0\\ 0 & 0 & 0 & 0 & 0 & N'_{w2}\end{bmatrix}, \tag{7}$$

$$\Delta\boldsymbol{u}^{\mathrm{e}} = [\Delta w_{Gi} \quad \Delta u_{si} \quad \Delta u'_{si} \quad \Delta v_{si} \quad -\Delta v'_{si} \quad \Delta\theta_{zi} \quad \Delta w_{Gj} \quad \Delta u_{sj} \quad \Delta u'_{sj} \quad \Delta v_{sj} \quad -\Delta v'_{sj} \quad \Delta\theta_{zj}]^{\mathrm{T}}. \tag{8}$$

According to Eq.(2), the linear strain can be expressed as

$$\Delta\boldsymbol{\varepsilon}_{\mathrm{L}} = \begin{Bmatrix}\Delta\varepsilon_{\mathrm{L}}\\ \Delta\gamma\end{Bmatrix} = \boldsymbol{B}_{\mathrm{L}}\Delta\boldsymbol{u}^{\mathrm{e}}, \tag{9}$$

in which $\boldsymbol{B}_{\mathrm{L}}$ is the linear strain matrix of the element

$$\boldsymbol{B}_{\mathrm{L}} = \begin{bmatrix}\dfrac{\partial}{\partial z} & 0 & -x\dfrac{\partial}{\partial z} & 0 & y\dfrac{\partial}{\partial z} & 0\\ 0 & 0 & 0 & 0 & 0 & K_\theta\end{bmatrix}\boldsymbol{N}. \tag{10}$$

Correspondingly, the nonlinear strain may be expressed as

$$\Delta\boldsymbol{\varepsilon}_{\mathrm{N}} = \{\Delta\varepsilon_{\mathrm{N}}\} = \frac{1}{2}\boldsymbol{A}^{\mathrm{T}}\boldsymbol{A}, \tag{11}$$

in which

$$\boldsymbol{A} = \boldsymbol{B}_{\mathrm{NL}}\Delta\boldsymbol{u}^{\mathrm{e}}, \tag{12}$$

where $\boldsymbol{B}_{\mathrm{NL}}$ is the nonlinear strain matrix of the element

$$\boldsymbol{B}_{\mathrm{NL}} = \begin{bmatrix}\dfrac{\partial}{\partial z} & 0\\ 0 & \dfrac{\partial}{\partial z}\end{bmatrix}\begin{bmatrix}0 & 1 & 0 & 0 & 0 & -(y-y_s)\\ 0 & 0 & 0 & 1 & 0 & x\end{bmatrix}\boldsymbol{N}. \tag{13}$$

The stress increment $\Delta\boldsymbol{\sigma}$ can be approximated using the linear strain increment as

$$\Delta\boldsymbol{\sigma} = \begin{Bmatrix}\Delta\sigma\\ \Delta\tau\end{Bmatrix} = \boldsymbol{D}\begin{Bmatrix}\Delta\varepsilon_{\mathrm{L}}\\ \Delta\gamma\end{Bmatrix} = \boldsymbol{D}\Delta\boldsymbol{\varepsilon}_{\mathrm{L}}, \tag{14}$$

where $\boldsymbol{D}$ is the material property matrix. Neglecting the influence of the shear strain, $\boldsymbol{D}$ can be expressed as

$$\boldsymbol{D} = \begin{bmatrix}E(\varepsilon) & 0\\ 0 & G\end{bmatrix}, \tag{15}$$

where $E(\varepsilon)$ is the tangent modulus of the material which is dependent on the strain state, and G is the elastic shearing modulus regarded as a constant.

According to the principle of virtual work, we have

$$\int_V (\boldsymbol{\sigma}+\Delta\boldsymbol{\sigma})\delta\Delta\boldsymbol{\varepsilon}\mathrm{d}V=\int_L (\boldsymbol{q}+\Delta\boldsymbol{q})\delta\Delta\boldsymbol{u}\mathrm{d}z+(\boldsymbol{P}+\Delta\boldsymbol{P})\delta\Delta\boldsymbol{u}, \tag{16}$$

in which $\boldsymbol{\sigma}$ and $\Delta\boldsymbol{\sigma}$ are the stress vector and stress increment of the current state, $\boldsymbol{q}$ and $\boldsymbol{P}$ are the distributed load and concentrated load vector, $\Delta\boldsymbol{q}$ and $\Delta\boldsymbol{P}$ are the increments of distributed load and concentrated load, $\delta\Delta\boldsymbol{u}$ and $\delta\Delta\boldsymbol{\varepsilon}$ are the virtual displacement and virtual strain, and V is the volume of the element. Substitute Eqs.(9), (11) and (14) into Eq.(16) and ignore the infinitesimal variable $\Delta\boldsymbol{\sigma}\Delta\boldsymbol{\varepsilon}_{\mathrm{N}}$, we have

$$(\boldsymbol{K}_{\mathrm{ep}}+\boldsymbol{K}_{\sigma})\Delta\boldsymbol{u}^{\mathrm{e}}=\Delta\boldsymbol{F}^{\mathrm{e}}, \tag{17}$$

where $\Delta\boldsymbol{F}^{\mathrm{e}}$ is the increment of element load vector corresponding to $\Delta\boldsymbol{u}^{\mathrm{e}}$, the element displacement vector. $\boldsymbol{K}_{\mathrm{ep}}$ and $\boldsymbol{K}_{\sigma}$ are the elasto-plastic and geometric stiffness matrixes of the beam element respectively as follows

$$\begin{cases}\boldsymbol{K}_{\mathrm{ep}}=\int_V \boldsymbol{B}_{\mathrm{L}}^{\mathrm{T}}\boldsymbol{D}\boldsymbol{B}_{\mathrm{L}}\,\mathrm{d}V,\\ \boldsymbol{K}_{\sigma}=\int_V \boldsymbol{G}^{\mathrm{T}}\boldsymbol{\sigma}\boldsymbol{G}\,\mathrm{d}V.\end{cases} \tag{18}$$

The distribution of elastic and plastic zones is non-uniform in the element, and varies during deformation. It is very difficult to present an explicit expression of the property matrix $\boldsymbol{D}$ for the whole section. Hence, the section is divided into many subareas, as shown in Fig.2, and the fiber model is adopted to calculate the element's stiffness matrix, i.e.

$$\boldsymbol{K}_{\mathrm{ep}}\approx\sum_{i=1}^{n}\left(\int_L \boldsymbol{B}_{\mathrm{L},i}^{\mathrm{T}}\boldsymbol{D}_i\boldsymbol{B}_{\mathrm{L},i}\Delta A_i\mathrm{d}x\right). \tag{19}$$

Obviously, if the number of subareas is sufficiently large, the result of Eq.(19) will approach the exact solution. The value of $\boldsymbol{K}_{\mathrm{ep}}$ is calculated using numerical integration, with $\boldsymbol{D}_i$ being regarded as constant in subarea ΔA_i.

To compute the geometric stiffness matrix $\boldsymbol{K}_{\sigma}$, the normal stress should be expressed in terms of axial force and bending moment, which actually has very little contribution to the geometric stiffness, so

$$\sigma=N/A, \tag{20}$$

where N is the axial force, and A is the sectional area.

Prestressing reinforcement element

The reinforced bars parallel to the beam axis may be regarded as fibers, whose contributions to the stiffness could be readily accounted for in Eq.(19). The contributions to the stiffness from those not parallel to the beam and the prestressing reinforcement (PR), will however be calculated in the following section.

The displacement increment of two ends of the prestressing reinforcement in Fig.3 can be expressed by Eq.(21):

$$\begin{cases}\Delta W_r^*=\Delta w_{G,r}-x_r\Delta u'_{s,r}-y_r\Delta v'_{s,r},\\ \Delta U_r^*=\Delta u_{s,r}-(y_r-y_s)\Delta\theta_{z,r},\\ \Delta V_r^*=\Delta v_{s,r}+x_r\Delta\theta_{z,r},\\ r=i,j,\end{cases} \tag{21}$$

where the subscripts i and j indicate the parameters of the corresponding section.

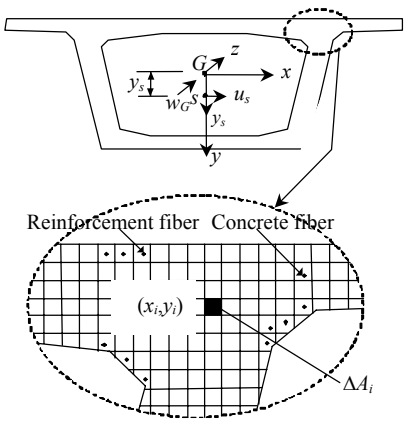

Fig.2 Division scheme of section

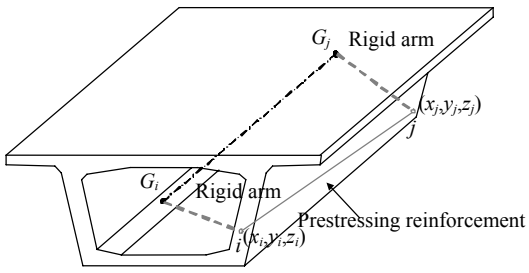

Fig.3 Location of prestressing reinforcement in girder

Ignoring the bending stiffness, the stiffness equation of PR can be expressed as

$$\left(\boldsymbol{k}_{\mathrm{ep}}^{*}+\boldsymbol{k}_{\sigma}^{*}\right)\Delta\boldsymbol{\delta}^{*}=\Delta\boldsymbol{f}^{*}, \tag{22}$$

in which $\boldsymbol{k}_{\mathrm{ep}}{}^{*}$ and $\boldsymbol{k}_{\sigma}{}^{*}$ are respectively the elasto-plastic and the geometric stiffness matrixes, $\Delta\boldsymbol{\delta}^{*}$ is the nodal displacement vector, and $\Delta\boldsymbol{f}^{*}$ is the nodal force vector of the prestressing reinforcement element in the local coordinate system. According to Fig.4, $\Delta\boldsymbol{\delta}^{*}$ and $\Delta\boldsymbol{f}^{*}$ can be written in the form

$$\begin{cases}\Delta\boldsymbol{\delta}^{*}=\left[\Delta W_i^{*} \quad \Delta U_i^{*} \quad \Delta V_i^{*} \quad \Delta W_j^{*} \quad \Delta U_j^{*} \quad \Delta V_j^{*}\right]^{\mathrm{T}},\\ \Delta\boldsymbol{f}^{*}=\left[\Delta f_{zi}^{*} \quad \Delta f_{yi}^{*} \quad \Delta f_{xi}^{*} \quad \Delta f_{zj}^{*} \quad \Delta f_{yj}^{*} \quad \Delta f_{xj}^{*}\right]^{\mathrm{T}}.\end{cases} \tag{23}$$

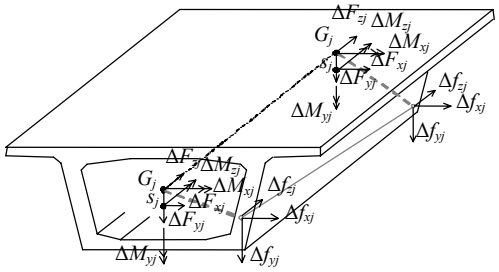

Fig.4 Translation of the prestressing reinforcement

As PR is bonded with concrete, the deformation of PR can be transformed by that of the girder element by

$$\Delta\boldsymbol{\delta}^{*}=\begin{bmatrix}\boldsymbol{B}_i^{\mathrm{T}} & \boldsymbol{0}\\ \boldsymbol{0} & \boldsymbol{B}_j^{\mathrm{T}}\end{bmatrix}\Delta\boldsymbol{u}^{\mathrm{e}}, \tag{24}$$

in which

$$\boldsymbol{B}_r^{\mathrm{T}}=\begin{bmatrix}1 & 0 & -x_r & 0 & y_r & 0\\ 0 & 1 & 0 & 0 & 0 & -(y_r-y_s)\\ 0 & 0 & 0 & 1 & 0 & x_r\end{bmatrix},\ (r=i,j). \tag{25}$$

The nodal force of PR also should be translated to that of the girder element by

$$\Delta\boldsymbol{f}^{*}=\begin{bmatrix}\boldsymbol{B}_i^{\mathrm{T}} & \boldsymbol{0}\\ \boldsymbol{0} & \boldsymbol{B}_j^{\mathrm{T}}\end{bmatrix}\Delta\boldsymbol{F}^{\mathrm{e}}. \tag{26}$$

Then, the elasto-plastic stiffness matrix of PR element in the coordinate system of the beam element can be obtained as

$$(\tilde{\boldsymbol{k}}_{\mathrm{ep}}+\tilde{\boldsymbol{k}}_{\sigma})\Delta\boldsymbol{u}^{\mathrm{e}}=\Delta\boldsymbol{F}^{\mathrm{e}}, \tag{27}$$

where

$$\tilde{\boldsymbol{k}}_{\mathrm{ep}}=\begin{bmatrix}\boldsymbol{B}_i & \boldsymbol{0}\\ \boldsymbol{0} & \boldsymbol{B}_j\end{bmatrix}\boldsymbol{k}_{\mathrm{ep}}^{*}\begin{bmatrix}\boldsymbol{B}_i & \boldsymbol{0}\\ \boldsymbol{0} & \boldsymbol{B}_j\end{bmatrix}^{\mathrm{T}}, \tag{28}$$

$$\tilde{\boldsymbol{k}}_{\boldsymbol{\sigma}}=\begin{bmatrix}\boldsymbol{B}_i & \boldsymbol{0}\\ \boldsymbol{0} & \boldsymbol{B}_j\end{bmatrix}\boldsymbol{k}_{\boldsymbol{\sigma}}^{*}\begin{bmatrix}\boldsymbol{B}_i & \boldsymbol{0}\\ \boldsymbol{0} & \boldsymbol{B}_j\end{bmatrix}^{\mathrm{T}}. \tag{29}$$

Then the stiffness matrix $(\tilde{\boldsymbol{k}}_{\mathrm{ep}}+\tilde{\boldsymbol{k}}_{\boldsymbol{\sigma}})$ of the reinforcement can be added to the beam stiffness matrix accordingly.

CFST arch rib, steel girder or steel-concrete girder element

The fiber model mentioned above can also be used to simulate the CFST arch rib, steel stiffening girder or steel-concrete composite stiffening girder, with similar elasto-plastic stiffness matrix and stiffness equation. The detailed description of the deduction can be found in (Xie *et al.*, 2005).

However, for the CFST arch rib, the stress-strain relation of structure is very complex due to the combined influence of the confined concrete and outer steel tube. In this paper, the following stress-strain relation considering the confinement effect of the steel tube ring (Han, 2000) is adopted:

$$\sigma=\sigma_0(\varepsilon/\varepsilon_0)[2.0-K-(1-K)(\varepsilon/\varepsilon_0)],\ \varepsilon\le\varepsilon_0, \tag{30a}$$

$$\sigma=\begin{cases}\sigma_0(1-q)+\sigma_0 q(\varepsilon/\varepsilon_0)^{0.1\xi}, & \xi\ge 1.12;\\ \sigma_0(\varepsilon/\varepsilon_0)/[\beta(\varepsilon/\varepsilon_0-1)^2+\varepsilon/\varepsilon_0], & \varepsilon>\varepsilon_0,\\ & \xi<1.12,\end{cases} \tag{30b}$$

where σ and ε are the longitudinal compressive stress and strain respectively, and

$$\begin{aligned}&\sigma_0=f_{\mathrm{ck}}[1.194+(13/f_{\mathrm{ck}})^{0.45}(-0.07485\xi^2+0.5789\xi)],\\ &\varepsilon_0=\varepsilon_{\mathrm{c}}+(1400+40(f_{\mathrm{ck}}-20))\xi^{0.2},\ \varepsilon_{\mathrm{c}}=1300+14.93f_{\mathrm{ck}},\\ &K=0.1\xi^{0.745},\quad q=K/(0.2+0.1\xi),\quad \xi=\alpha f_{\mathrm{y}}/f_{\mathrm{ck}},\\ &\beta=5.0\times10^{-4}f_{\mathrm{ck}}^2(2.36\times10^{-5})^{0.25+(\xi-0.5)^7},\ \alpha=A_{\mathrm{s}}/A_{\mathrm{c}},\end{aligned} \tag{31}$$

where f_{ck} is the characteristic value of compressive strength of concrete (MPa), A_s is the area of steel tube (m^2), A_c is the area of concrete (m^2), and f_y is the yield strength of steel tube (MPa).

The interaction between the radial stress σ_r and the tangential stress σ_θ has been considered in calculation of the tensile and compressive strengths of the steel tube. According to the Von Misess yield criterion as shown in Fig.5a, we have

$$\sigma_z^2 - \sigma_z\sigma_\theta + \sigma_\theta^2 = f_y^2, \tag{32}$$

where σ_z is the axial normal stress of steel tube.

Substituting $\alpha=\sigma_\theta/f_y\approx0.159$ into Eq.(32), yields

$$\begin{cases}\sigma_{yt} = \beta_t f_y = 0.911 f_y,\\ \sigma_{yc} = \beta_c f_y = 1.07 f_y,\end{cases} \tag{33}$$

where σ_{yt} and σ_{yc} are the yield strengths of the tension and compression sides of the steel tube respectively, β_t and β_c are the corresponding coefficients. Fig.5b depicted the bilinear stress-strain relationship considering the hardening of the material.

The secondary modulus of the steel tube E_h, which is related to both material properties and the tendency of local buckling of the steel tube, is assumed to be 1% of the initial elastic modulus.

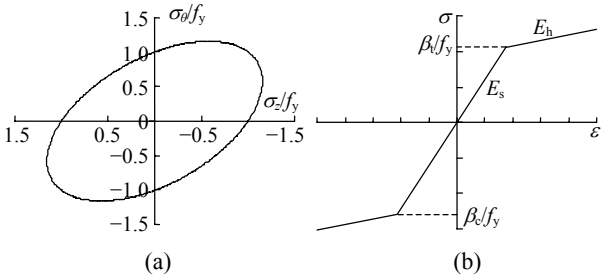

Fig.5 Stress-strain curves of steel tube
(a) Yield condition; (b) Stress-strain relationship

Hanger element

The mechanical behavior of cables such as that of hangers and tie bars, is similar to that of truss elements, except that cables cannot bear compressive forces and the initial sag will affect their stiffness. The elasto-plastic computation theory of flexible cable considering the effect of sag was presented by (Xie *et al.*, 1998). In most bridges, however, sag has little effect on the mechanical behavior of hangers. Hence, hangers of arch bridges are treated as elasto-plastic trusses with no compression strength, and the stiffness equation is expressed by Eq.(22).

PROGRAM SCHEME FOR ULTIMATE BEARING CAPACITY CALCULATION

As usual, a long-span CFST arch bridge is constructed by progressive erection without brackets, and consists of many construction stages. Thus, the function of simulating the construction process must be taken into account in the developed program for calculating ultimate bearing capacity, including the gradual action of load, the step-by-step formation of the structure, the influence of initial displacement and initial stress. The scheme for the program is indicated in Fig.6. The modified arc-length increment technique is adopted to solve the resulting nonlinear equation (Crisfield, 1981).

VALIDATION OF THE METHOD FOR A PC GIRDER

The accuracy of computation of the ultimate strength for CFST element has been confirmed in (Xie *et al.*, 2005). In this paper, the precision of the present theory is checked for a PC girder by comparison with the experimental result.

Fig.7 shows the cross-section and reinforcements of the girder, which spans 13 m, with 9 bundles of prestressing reinforcements and 11 branches of nonprestressing reinforced bars. The design strength of the concrete is 22.4 MPa, and those of nonprestressing reinforced bars A and B depicted in Fig.7a are 195 MPa and 280 MPa respectively of which the diameters are 12 mm and 8 mm. The prestressing reinforcement is high-strength low-relaxation steel strand with design strength of 1860 MPa and the control force of each bundle is N_k=195 kN. More detailed information about the experiment on this PC girder is available in (Chen, 2005).

Comparison of the deflection at the midspan is depicted in Fig.8, showing good consistency between the numerical simulation and experimental result.

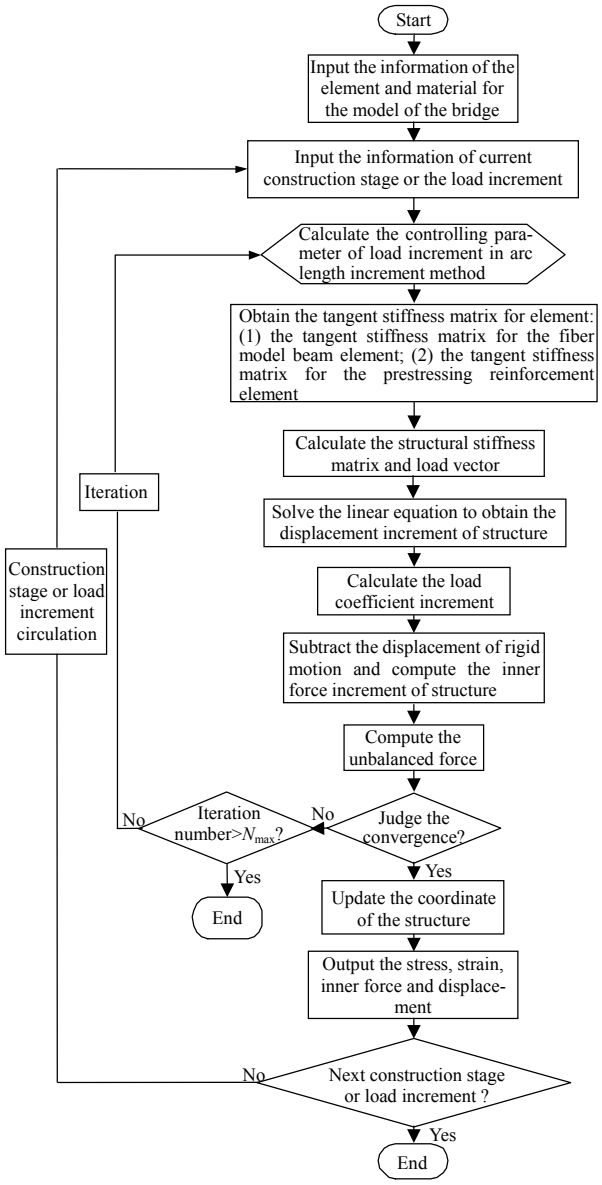

Fig.6 Program scheme for ultimate bearing capacity calculation

APPLICATION IN BRIDGE DESIGN

The ultimate strength of Fenghuajiang Bridge in Ningbo, Zhejiang, China is studied involving the effect of construction process to demonstrate the applicability of the present approach in bridge design. Fig.9 shows the design scheme of Fenghuajiang Bridge which is a girder and arch combination bridge

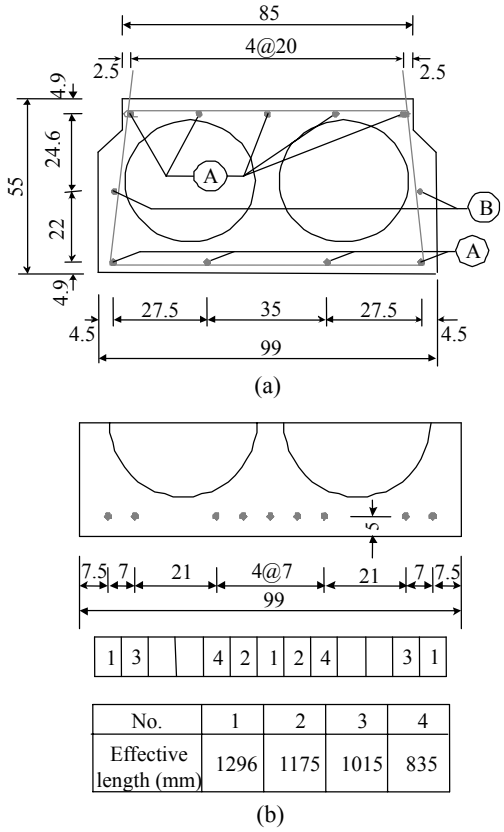

Fig.7 Cross-section and the reinforced bars of the girder (unit: cm). (a) Nonprestressing reinforced bars; (b) Prestressing reinforcements

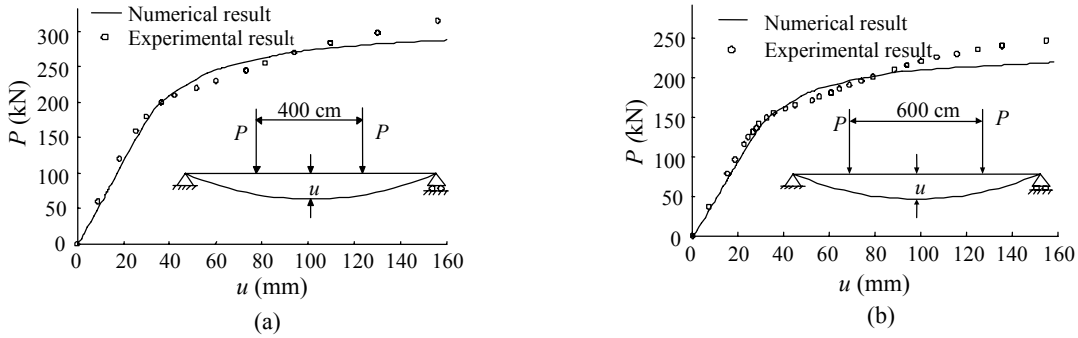

Fig.8 The comparison between the computation and the experimental result
(a) Load-deformation curves for Case I; (b) Load-deformation curves for Case II

with central span of 138 m. The central span of the stiffening girder is made up of steel and PC composite box. The side span of the stiffening girder is made up of PC box. The abnormal CFST arch in the central span is composed of three arches, with one main arch rib in the center and two secondary arch ribs. The diameter of the main arch rib is 1.8 m, and those of the other two are 1.5 m. The design strength of the concrete used in the bridge is 22.4 MPa. The arch ribs are linked with steel pipes and I-steel bearing members, forming a truss arch bridge. The main arch and the deck are connected with vertical hangers. The secondary arches and the deck are connected with inclined hangers.

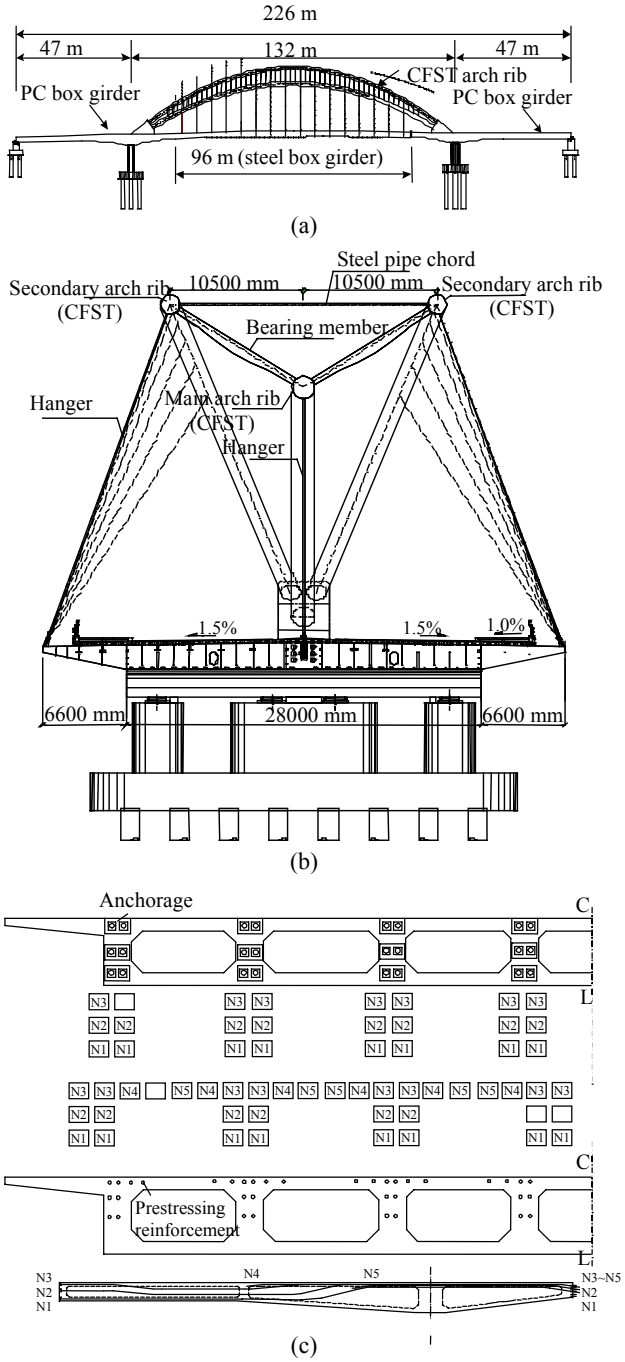

Fig.9 The design scheme of Fenghuajiang Bridge in Ningbo, China. (a) Elevation view; (b) The section of the mid span; (c) The section of the side span

To take into account the effect of the construction method on the ultimate bearing capacity, it is assumed that the bridge is constructed by two kinds of methods. In Case I, there is only a construction process, the supporting frames for construction falling once after the completion of the whole bridge. In Case II, there are two construction processes, as shown in Fig.10. The first process is construction of the PC girder on the supporting frames. The second process is to fix the steel girder, assemble the arch rib, and tension the tie-bar and hangers to separate the steel girder from the frame.

Prestressing reinforcements in the girder are properly simulated in construction stages, but the reinforced bars are not modelled due to their large number. The elasto-plastic mechanical behaviors of CFST arch ribs, hanger, bearing member, steel pipe, tie-bar, etc. are analyzed.

The ultimate strength analysis process is shown in Fig.11. First, the initial stress of the established bridge is calculated under dead load and prestressing force including initial tension of the hangers, the tie and prestressing reinforcements. Then the stress and displacement under live load are computed. At last,

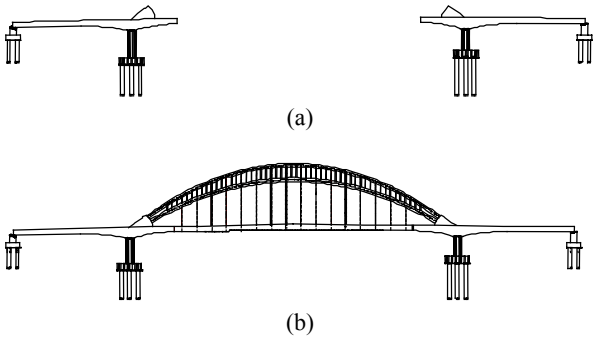

Fig.10 Construction process of Case II. (a) Construct the PC box, girder on frame (first process); (b) Fix the CFST arch ribs, the steel girders, the hangers and the tie-bar (second process)

the ultimate strength is investigated for load proportionally exerted on the bridge by the arc length increment method. The initial state of each step is based on the result of the last step.

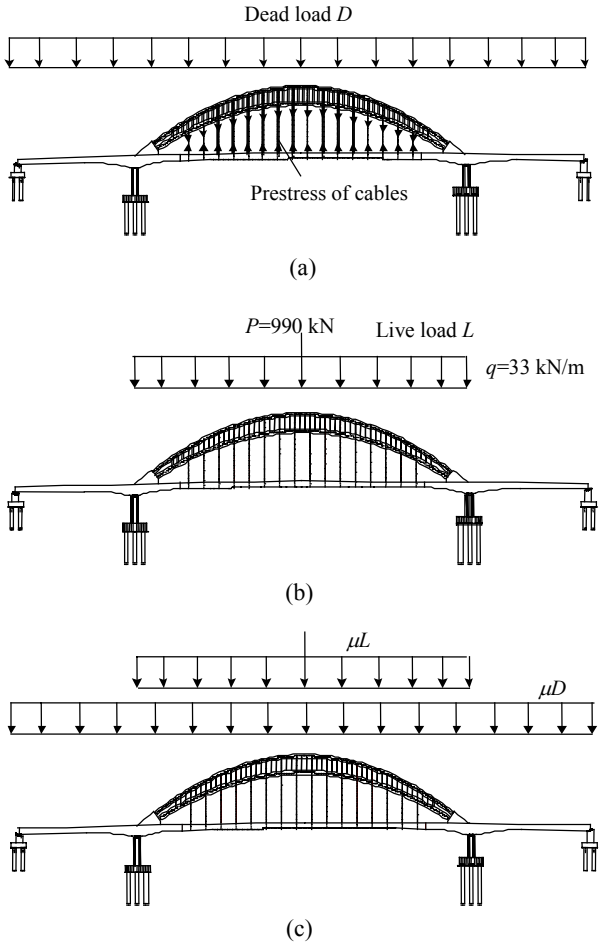

Fig.11 Approach of stability analysis of CFST arch bridge. (a) Calculate the initial stress of the completed bridge under dead load and prestressing; (b) Calculate the internal force and deformation under the live load; (c) Calculate the ultimate strength of the bridge

The influence of construction method on the initial internal forces is investigated. The axial force and bending moment of the main arch rib are shown in Fig.12, showing that the initial internal forces of the two construction methods differ with a relative error of 10% for the axial force (Fig.12a) and 25% for bending moment (Fig.12b).

The buckling modes for the two construction methods are depicted in Fig.13. The bridge is primarily subjected to vertical loads, so the deformation is mainly in the vertical plane. However, in order to obtain out-of-plane buckling modes, a small out-of-plane initial displacement is set to simulate the erection error. It is observed that the buckling modes for the two methods are quite similar.

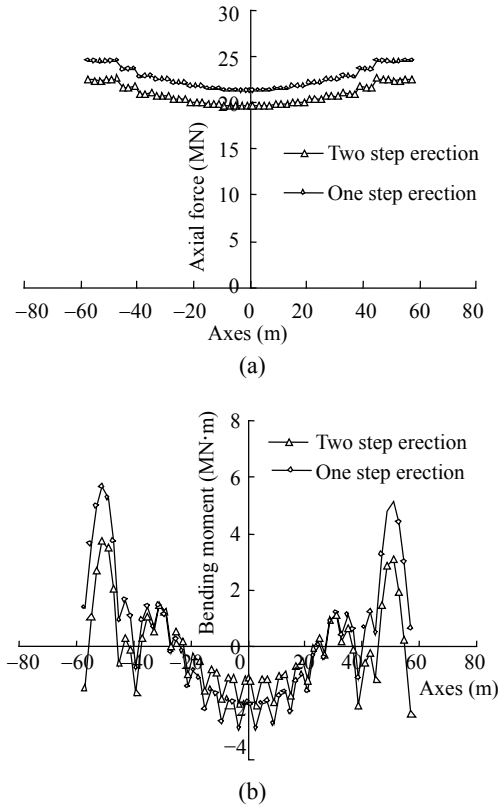

Fig.12 Longitudinal distributions of the initial internal forces in the mid arch for two cases. (a) Axial force; (b) Bending moment

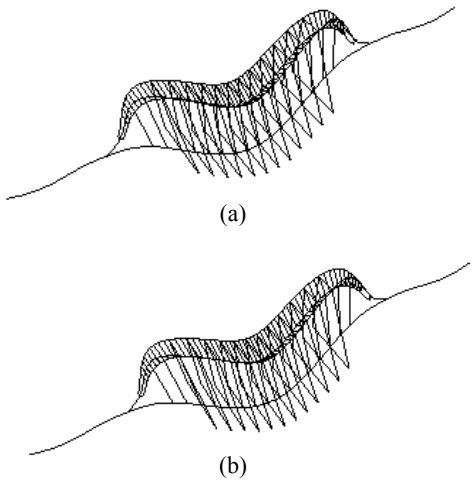

Fig.13 Buckling modes of the bridge
(a) Buckling mode for Case I; (b) Buckling mode for Case II

The out-of-plane deformation curves at the quarter points of the main arch rib are shown in Fig.14. The vertical axis denotes the load coefficient μ which does not contain the original dead load and live load exerted in Figs.11a and 11b. When $3.1 \leq \mu \leq 3.2$, the nonlinear behavior of the arch rib becomes obvious in the lateral direction. As shown in the figure, the buckling modes in both cases are antisymmetric out-of-plane, and the buckling load factor of the arch rib is about 4.1 considering the initial dead and live load.

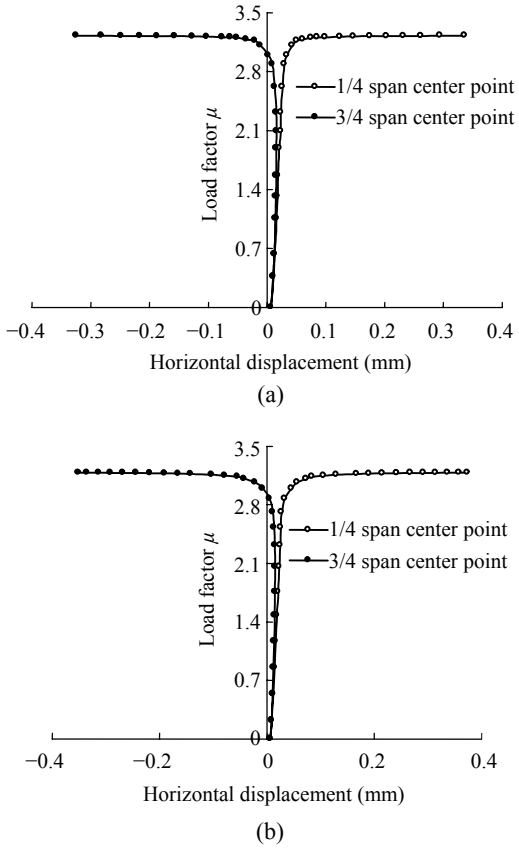

Fig.14 Out-of-plane deformation curves of the main arch rib. (a) Out-of-plane deformation in Case I; (b) Out-of-plane deformation in Case II

A comparison of the lateral and vertical deformations at the quarter point of the main arch between two cases is shown in Fig.15, showing that the deviation of the load-displacement curves of the two cases is very small, indicating that the influence of the construction method on the stability strength is very slight. Besides, when out-of-plane buckling occurs, the bridge still has certain vertical stiffness.

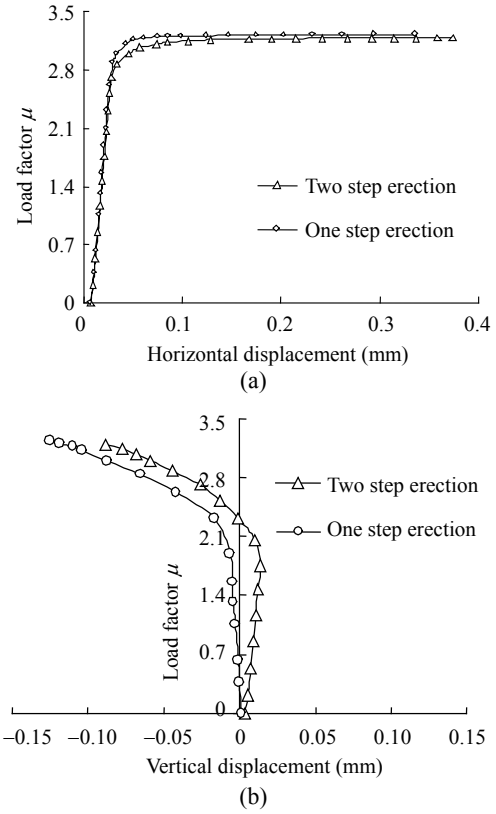

Fig.15 Load-deformation curves comparison between two cases. (a) Lateral deformation at the quarter point of the mid arch; (b) Vertical deformation at the quarter point of the mid arch

CONCLUSION

In analyzing the ultimate strength of the CFST arch bridges with stiffening girders, simulating the nonlinear behavior of stiffening girders is as important as that of the CFST arch rib due to the redistribution of inner force between arch ribs and stiffening girders. In this paper, an analytical approach for estimating the ultimate bearing capacity of CFST arch bridge with stiffening girder is proposed, which takes account of the effects of material and geometric nonlinearity and the contribution of prestressing reinforcement. Based on the fiber beam element theory, the degrees of freedom of the whole structure can be reduced, making it very feasible to predict the ultimate strength of the complex structure. The accuracy of the present method was examined by comparison with the experimental results for a PC girder.

To demonstrate the applicability of the present

approach in bridge design, the ultimate strength of an abnormal CFST arch bridge with stiffening girder is studied considering the effect of construction process. The result shows that the construction process influences the initial internal force of the bridge significantly. But it has little effect on the ultimate strength of the bridge. Therefore, the relatively accurate stability strength can be obtained by ignoring the influence of the construction process.

References

Chen, H.Z., 2005. Research of Calculation and Analysis of PC Box Girder Structure with Long Span. Ph.D Thesis, Zhejiang University (in Chinese).

Chen, B.C., Chen, Y.J., 2000. Experimental study on mechanic behaviors of concrete-filled steel tubular rib arch under in-plane loads. *Engineering Mechanics*, **17**(2):44-50 (in Chinese).

Chen, B.C., Wei, J.G., Lin, J.Y., 2006. Experimental study on concrete filled steel tubular (single tube) arch with one rib under spatial loads. *Engineering Mechanics*, **23**(5):99-106 (in Chinese).

Crisfield, M.A., 1981. A fast incremental iterative solution procedure that handles "snap through". *Computer and Structures*, **13**(1-3):55-62. [doi:10.1016/0045-7949(81)90108-5]

Cui, J., Sun, B.N., Lou, W.J., Yang, L.X., 2004. Model test study on concrete-filled steel tube truss arch bridge. *Engineering Mechanics*, **21**(5):83-86 (in Chinese).

Han, L.H., 2000. Steel Tube Confined Concrete Structures. Science Press, Beijing, p.180-190 (in Chinese).

Hu, Q.A., Zhou, X. S., Zhu, H., 2006. Impacts of Poisson ratio on ultimate bearing capacity of concrete filled steel tubular arch bridge. *Chinese Journal of Applied Mechanics*, **23**(1):128-131 (in Chinese).

Xie, X., Nagai, M., Yamaguchi, H., 1998. Ultimate strength analysis of long-span cable-stayed bridges. *Journal of Structural Mechanics and Earthquake Engineering, JSCE*, **598**(I-44):171-181 (in Japanese).

Xie, X., Chen, H.Z., Li, H., Song, S.R., 2005. Numerical analysis of ultimate strength of concrete filled steel tubular arch bridges. *Journal of Zhejiang University SCIENCE*, **6A**(8):859-868. [doi:10.1631/jzus.2005.A0859]

Zeng, G.F., Fan, L.C., Zhang, G.Y., 2003. Load capacity analysis of concrete filled steel tube arch bridge with the composite beam element. *Journal of the China Railway Society*, **25**(5):97-102 (in Chinese).

Zhang, Z.A., Sun, Y., Wang, M.Q., 2003. Key technique in the erection process of the rib steel pipe truss segments for Wushan Yangze River bridge. *Highway*, **12**:26-32 (in Chinese).

Zhang, Y., Shao, X.D., Cai, S.B., Hu, J.H., 2006. Spatial nonlinear finite element analysis for long-span trussed CFST arch bridge. *China Journal of Highway and Transport*, **19**(4):65-70 (in Chinese).

Zhao, L.Q., Xu, R.H., Zheng, X.Z., 2004. Overall design of the fourth Qiantangjiang River Bridge in Hangzhou. *Bridge Construction*, **1**:27-30 (in Chinese).